Isı Bilimi ve Tekniği Dergisi, 34, 1, 123-135, 2014
J. of Thermal Science and Technology

ISSN 1300-3615

SITE-SPECIFIC OPTIMIZATION OF A SMALL-SCALE HORIZONTAL AXIS WIND TURBINE VIA MICRO GENETIC ALGORITHM

Emre ALPMAN[*], M. Onur KIMILLI[**], Abdullah ERİŞİK[***], Erdi ŞAHİN[****]
[1]Marmara University, Mechanical Engineering Department, Kadıköy, Istanbul, Turkey, 34722.
[*]Corresponding author, emre.alpman@marmara.edu.tr
[**]onurkimilli@hotmail.com
[***]a.erisik@hotmail.com
[****]erdisahin88@hotmail.com

(Geliş Tarihi: 08.03.2013 Kabul Tarihi: 26.04.2014)

Abstract: Optimization of 10.6m diameter, constant speed and stall regulated horizontal axis wind turbine was performed for Gökçeada location in Turkey using a genetic algorithm. Optimizations were performed by maximizing the annual energy production of the turbine which was calculated using a blade element momentum theory code. Predictions by the code were validated by comparing them with experimental data and computational fluid dynamics solutions obtained using different turbulence models. Chord length and twist angle distributions along the blade span, airfoil profiles for the root, primary and tip sections of the blades, and pitch angle of the blades were used as design parameters. A micro-genetic algorithm with a population size of five individuals was used for the optimizations. Two- and three-bladed turbines were considered for rated power of 20 and 30 kW. Optimizations performed for 5000 generations showed that two-bladed turbines could produce as much energy as three-bladed ones at the expense of rotating faster and experiencing higher blade loading. By having a lower solidity, however, two-bladed designs produced lower thrust forces.
Keywords: Horizontal axis wind turbine optimization, micro-genetic algorithm, blade element momentum theory, computational fluid dynamics, annual energy production.

KÜÇÜK ÖLÇEKLİ YATAY EKSENLİ BİR RÜZGAR TÜRBİNİNİN MİKRO GENETİK ALGORİTMA KULLANILARAK BÖLGEYE ÖZGÜ OPTİMİZASYONU

Özet: Türkiye' deki Gökçeada bölgesi için 10.6m çapında, sabit hızlı ve tutunma kaybına göre düzenlenmiş yatay eksenli rüzgâr türbini optimizasyonu, genetik algoritma kullanılarak yapılmıştır. İyileştirmeler, türbinin yıllık enerji üretimini maksimuma çıkarmak suretiyle gerçekleştirilmiştir. Enerji üretimi için kanat elemanı momentum teorisini uygulayan bir kod kullanılmıştır. Kodun tahminleri, deneysel veriler ve farklı türbülans modelleri kullanan hesaplamalı akışkanlar dinamiği çözümleri ile karşılaştırılarak doğrulanmıştır. Kanat açıklığı boyunca yeter uzunluğu ve burkulma açısı dağılımı, kanadın kök, ana ve uç kısımları için kanat kesiti profilleri ve kanadın yunuslama açısı tasarım parametreleri olarak kullanılmıştır. Optimizasyonlar, nüfus büyüklüğü beş birey olan bir mikro-genetik algoritma kullanılarak gerçekleştirilmiştir. 20 ve 30 kW' lık nominal güç değerleri için iki ve üç kanatlı konfigürasyonlar değerlendirilmiştir. 5000 kuşak boyu yapılan iyileştirmeler göstermiştir ki, iki kanatlı bir türbin, daha hızlı dönmek ve kanatların daha çok yüklenmesi pahasına, üç kanatlı bir türbin kadar enerji üretebilir. Bununla birlikte, daha düşük katılık oranına sahip iki kanatlı tasarım, daha düşük itme kuvveti üretmiştir.
Anahtar Kelimeler: Yatay eksenli rüzgar türbini optimizasyonu, mikro-genetik algorithm, kanat elemanı momentum teorisi, hesaplamalı akışkanlar dinamiği, yıllık enerji üretimi.

INTRODUCTION

Increasing global warming and environmental pollution forced the nations resort to renewable energy sources like wind energy. However, due to the constantly increasing energy demand of the world, the clean energy should also be obtained efficiently. Wind energy is obtained using devices called wind turbines which convert the kinetic energy of the wind to mechanical energy. Rotation of a wind turbine is caused by the aerodynamic forces developing on the blades. Therefore, aerodynamic design of the blades is very important to maximize the energy capture (Burton et al. 2001). Wind turbine blades are designed for maximum power production at low cost, which is achieved by searching for suitable turbine parameters which minimize the cost of energy. In references (Fuglsang, and Madsen, 1999) and (Fuglsang, and Thomsen, 2001), wind turbine design was performed using gradient based search algorithms. These

algorithms however, are successful for smooth search spaces containing a single extreme (Holst, 2005). Genetic algorithms, on the other hand, are gradient-free optimization methods which try to mimic natural evolution process. Being gradient-free they are very insensitive to the presence of local extremes in the search space (Holst, 2005) hence they are very suitable for multi-parameter optimization problems like wind turbine design. In optimization with a genetic algorithm, a group of turbines called a population is generated and each individual turbine is evaluated according to its fitness function, which may be the power output or the cost of energy. The individuals with low fitness values are eliminated and replaced by new individuals (children) created by crossing-over the properties of selected parent individuals. This way a new generation is produced. The individuals of this generation are then evaluated and the procedure continues until the population converges or the maximum number of generations is reached (Holst, 2005). Examples of wind turbine design using genetic algorithms can be found in references (Giguére and Selig, 1999; Eke and Onyewuidala, 2010; Diaz-Casas et al. 2012; Ceyhan, 2008; Sagol, 2010). Since the survivability of the individuals is determined by the fitness function, its evaluation is very crucial in a genetic algorithm. In wind turbine design, the fitness function is directly related to the power output of the turbine which is generated by the aerodynamic forces developing on the blades. Therefore, accurate simulation of flow over a wind turbine becomes very important for the design process. A wind turbine typically operates under unsteady wind conditions. The wind direction is also yawed with respect to the rotation axis most of the time (Leishman, 2002). This leads to a complicated flow field which could be predicted accurately by numerically solving Navier-Stokes equations with a suitable turbulence model. Such computational fluid dynamics (CFD) approach would require millions of grid points (Sorensen et al. 2002; Duque et al. 2003; Tachos et al. 2009) and hours of CPU time even with today's computing power. Moreover, the selected turbulence model would also affect the accuracy of the solution (Benjanirat and Sankar, 2003). In addition to this, wind turbine design using a genetic algorithm would require such CFD solutions to be performed for all the turbines in the population separately. Such solutions should be repeated at each generation, and this would be extremely costly. Quick load predictions can be obtained using blade element momentum theory (BEMT) (Burton et al. 2001; Leishman, 2002). Despite its weaknesses for high wind speeds, unsteady conditions and yaw error, it can yield good predictions for steady wind conditions (Leishman, 2002). This makes it a very suitable tool for preliminary calculations performed to rank the individuals in the population (Diaz-Casas et al. 2012). Hence BEMT has been often used for wind turbine design using genetic algorithms (Giguére and Selig, 1999; Eke and Onyewuidala, 2010; Diaz-Casas et al. 2012; Ceyhan, 2008; Sagol, 2010).

Wind characteristics of a wind turbine site are also very crucial for the performance of the turbines located there (Burton et al. 2001). Therefore a site-specific optimization (Fuglsang, and Thomsen, 2001; Diaz-Casas et al. 2012; Sagol, 2010) should be performed for maximum energy capture, which is the focus of this study. Here, aerodynamic optimization of a 10.6 m diameter horizontal axis wind turbine was performed for Gökçeada location in Turkey. According to the International Standard for design requirements for small wind turbines (IEC 61400-2, 2006), a turbine with a rotor area below 200 m^2 and a rated power below 50 kW is considered to be a small-scale wind turbine (World Wind Energy Association, 2012). A turbine of this size is too small to be part of a wind farm. However; it can be used for house-hold applications or in farms for water pumping, etc (World Wind Energy Association, 2012). Moreover, this diameter is same with that of NREL Phase VI turbine (Giguére and Selig, 1999), which has abundant experimental data (Simms et al. 2001). Also, according to laws of Turkish Republic, energy production less than 500 kW can be done without requiring an official license.

METHODOLOGY

Site-specific optimization of a 10.6m diameter, stall regulated and constant speed wind turbine was performed for Gökçeada, Turkey using a genetic algorithm. For this purpose, an open source genetic algorithm code written by David L. Carroll (http://www.cuaerospace.com/carroll/ga.html) was used. Here the annual energy production (AEP) was selected as the fitness function, and the code was updated accordingly. Usually, the cost of energy, defined as the ratio of total cost to AEP (Fugslang and Madsen, 1999), has been used in the literature as fitness function for wind turbine design (Fugslang and Madsen, 1999; Fuglsang and Thomsen, 2001; Eke and Onyewuidala, 2010; Diaz-Casas et al. 2012; Sagol, 2010). However, reliable cost models were typically defined for turbines with a diameter greater than 20m. Therefore, AEP was adhered to as the fitness function in this study.

In order to calculate AEP of a turbine, the variation of power generated with wind speed and the wind characteristics of the turbine site are needed. The latter was obtained using Weibull distribution of wind (Burton et al. 2001) for Gökçeada location (Sagol, 2010). For the calculation of the power output of turbines at different wind speeds, the BEMT solver WT_Perf (http://wind.nrel.gov/designcodes/simulators/wtperf) was used. This solver was developed by National Renewable Energy Laboratory (NREL), operated by the Alliance for Sustainable Energy, LLC for the U.S. Department of Energy. During the computations, drag force was included in the axial and tangential induction factor calculations. Prandtl hub and tip loss corrections (Burton et al. 2001) were included along with swirl effects. The rotor was

Table 1. Airfoil Database

Portion	Airfoils
Root	FFA-W3-241, FFA-W3-301, NACA 63-430, S814, S823
Primary	FFA-W3-211, FFA-W3-241, FX-66-S196, NACA 63-218, NACA 63-221, NACA 64-421, NACA 65-421, S809, S822, S834
Tip	Airfoils for primary portion + SD2030, NACA 63-215, NACA 64-415, NACA 65-415, FX-63-137, E387.

assumed to have no precone angle, shaft tilt or yaw error.

The optimization parameters for blade design were selected as chord length and twist angle distributions along the blade span, the pitch angle of the blades and airfoil profiles for the root, primary and tip portions of the blades. For chord and twist distributions, the procedure described in (Sagol, 2010) was followed by defining them using second order polynomials. Therefore, a total number of six design parameters were defined in order to describe chord and twist distributions. In addition to this, three parameters for the airfoil sections and one parameter for the blade pitch angle led to a total of ten design parameters.

In order to find a suitable rotation speed for the turbine, the optimal tip speed ratio (λ) was needed. Therefore, for a given individual turbine geometry and pitch angle, power coefficient (Cp) versus λ distribution was obtained by running WT_Perf for different wind speeds. Here, the rotation speed was taken as 72 rpm (see Simms et al. 2001). Then, the λ corresponding to maximum Cp was taken as the optimal tip speed ratio. The corresponding rotation speed was calculated by multiplying the optimal tip speed ratio with the mean wind speed (Burton et al. 2001) and then dividing with the rotor radius. The power output for the turbine was obtained for wind velocities between 4 m/s and 25 m/s by running WT_Perf one more time. The corresponding AEP was calculated using the Weibull distribution for the wind speed (Sagol, 2010: Kimilli et al. 2012). Here the wind velocities 4m/s and 25 m/s were taken as the cut-in and the cut-out wind speeds of the turbine studied. The AEP values presented in this study assumed that the turbine operated at full capacity for the whole year. While this is not a realistic situation, the AEP predictions were only used for ranking purposes.

BEMT requires the aerodynamic data (lift and drag coefficients versus angle of attack) of the airfoil used at a segment on the blade at different Reynolds numbers (Burton et al. 2001). For this study, an airfoil database for WT_Perf was created. The selection of airfoils for the root, primary and the tip portions of the blade was added as design parameters. The root section extended up to 0.4R, the primary portion covered the region between 0.4R and 0.9R, and the tip region constituted the rest of the blade. Here R was the rotor radius measured from the rotation axis. The airfoils in the database can be seen in Table 1. While the database was being generated, airfoils which had more than 24% thickness were allocated for the root section while airfoils with thicknesses between 18% and 24 % were reserved for the primary portion of the blade. Tip airfoils included the primary airfoils plus thinner airfoils. During the computations it was found that the Reynolds number was changing between 0.5×10^6 and 1.5×10^6 across the blade span. Therefore, aerodynamic data of the airfoil in this Reynolds number range was required. These data was mainly acquired from wind tunnel measurements (Selig et al. 1995; Selig and McGranahan,2004; wind.nrel.gov/airfoils/Coefficients) performed for the airfoils in the database. Wind tunnel data for the NACA profiles mentioned in Table 1 were available at Reynolds number of 3×10^6 (Bertagnolio et al. 2001). Therefore, aerodynamic data at the desired Reynolds number range were generated using the XFLR5 software (http://www.xflr5.com/xflr5.htm). Here predictions were obtained using fixed transition to turbulence which was set at 2% chord on the upper surface and 5% chord on the lower surface (WindPACT, 2003). This fixed transition approach was followed in order to include the roughness effect which typically occurs due to leading edge contamination (Somers, 2005). The XFLR5 software uses the X-Foil solver for computations (http://web.mit.edu/drela/Public/web/xfoil). X-Foil predictions obtained at Reynolds number of 3 million for the NACA profiles in the database showed good agreement with experimental data (Bertagnolio, 2001) up to 10 degrees of angle of attack. Beyond this value predictions were shown to deviate considerably from measurements. Therefore, aerodynamic data for NACA profiles were generated for angles of attack between 0 and 10 degrees.

WT_Perf required the aerodynamic data for angles of attack ranging from -180 ° to 180°. In order to extrapolate aerodynamic data to this range, the preprocessor program AirfoilPrep, which was developed at NREL (Hansen, 2012), was used. AirfoilPrep used Viterna method for the extrapolation. The program was also used to implement corrections to post stall data of airfoils due to three-dimensional effects.

Quality of a BEMT solution is also affected by the number of segments used on the blade. Therefore, a segment independence study was performed on the WT_Perf solutions. Here, AEP of the turbines in a population of five were calculated using 8, 16, 32, 64 and 128 segments on a blade. The blade parameters and wind conditions were kept same for all cases. The results were represented in Figure 1 where the AEP predictions showed considerable changes at low number of segments nevertheless they stabilized as this number increased. Doubling the segment number also doubled the computational time for the predictions. Therefore, looking at the predictions in Figure 1 and

the CPU times spent, 64 segments was decided to be sufficient and used through the rest of the study.

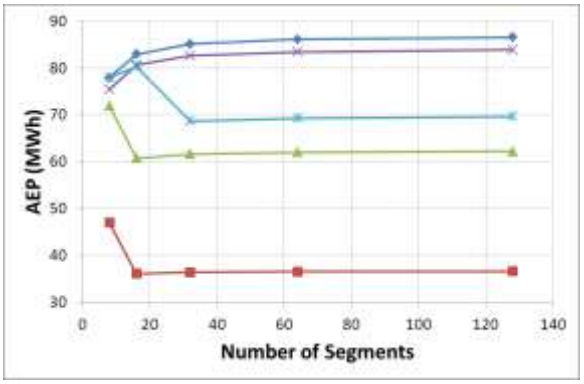

Figure 1. AEP of the turbines in a population of five. Calculated using 8, 16, 32, 64 and 128 segments (from bottom to top) on a blade

Optimization procedure was performed using the micro-genetic algorithm technique (Senecal, 2000) which allows small size populations and results can be achieved faster. In the micro-genetic algorithm approach described in (Senecal, 2000) the population consists of five individuals. The algorithm uses an elitist strategy where the best individual is carried to next generation and the other four individuals are determined through selection and cross-over. Mutation is not applied; instead the convergence of the population is checked. If the population converges, four of the five individuals are regenerated randomly while keeping the best individual. This way sufficient diversity can be achieved (Senecal, 2000). This micro-genetic algorithm approach was used in this study along with tournament selection and uniform cross-over with a probability of 0.5 (Weise, 2009). Optimization was performed for two- and three-bladed turbine configurations with a prescribed rated power. Here the power generated by the best individual was not allowed to exceed 10% of this rated power. The optimization process continued until a maximum number of generations is reached, which was selected to be 5000. The flowchart of the optimization process is given in Figure 2.

In the genetic algorithm code (http://www.cuaerospace.com/carroll/ga.html) the values of the design parameters in their specified range are defined using a prescribed number of binary digits (bits). Here, the ten design parameters were represented using a total number of 68 bits. 15 of these bits were used for chord distribution, 33 of them were used for twist distribution, 14 of them were used for airfoil sections and 6 of them were used for the blade pitch angle. Since each bit can either be 1 or 0, n bits can represent 2^n values of a parameter in its specified range.

Convergence is checked by counting the number of different bits from the best individual and if this number is less than 5% of the total number of the bits then population is assumed to converge and population is randomly regenerated while keeping the best individual. Optimization performed using this strategy, however, leaded to the premature convergence of the best individual. The problem here was the four individuals apart from the best one became identical. Although the number of different bits remained above 5%, selection and cross-over continuously yielded the same individuals. Instead of increasing the limit of 5% or changing the population size, an alternative approach was followed in this study. Here, the regeneration process was performed at every ten generations whether or not convergence was achieved. The evolution of AEP of a three-bladed turbine with a rated power of 30kW obtained using these two strategies are displayed in Figure . According to this figure regenerating the population at every 10 generations clearly resulted in a much better turbine. In fact the AEP predictions with the original approach showed improvement during the first ten generations then they remained constant. Due to these reasons the alternative approach described above was used through the rest of the study.

VALIDATION OF BEMT

Despite its speed for load calculations, the weaknesses of BEMT for wind turbine aerodynamics are long known (Leishman, 2002). In order to see the performance of WT_Perf in load calculations, torque predictions of the code for the two-bladed NREL Phase VI turbine at different wind speeds was compared with experimental measurements (Simms et al. 2001) along with CFD predictions obtained using FINE-TURBO package of Numeca software (http://www.numeca.com/index.php?id=turbomachine). CFD solutions were obtained by solving Navier-Stokes equations using different turbulence models; Spalart-Allmaras (Spalart and Allmaras, 1992), standard k-ε (Launder and Sharma, 1974), k-ω SST (Menter, 1994), and low-Re k-ε model by Launder and Sharma (Launder and Sharma, 1974).

For the CFD simulations a block structured mesh was constructed using AutoGrid5 package of Numeca (http://www.numeca.com/index.php?id=turbomachine). Grid was constructed around one blade and periodic boundary conditions were applied at the relevant boundaries. The inflow boundary was located at five blade radii upstream of the rotor while the outflow boundary was located at ten blade radii downstream. The external boundary was five blade radii away from center of rotation.

No-slip adiabatic wall conditions were imposed on the solid boundaries along with a wall model for turbulence (http://www.numeca.com/index.php?id=turbomachine). Wind speed, air density and viscosity were specified at the inflow boundary. The relevant values were obtained from Table I of (Sorensen et al. 2002). Inflow conditions for turbulence intensity and dissipation were specified according to the guidelines specified at (FINE^{TM}/Turbo v8.7 User Manual, 2010) for external flows. Pressure was specified at the outflow boundary and farfield boundary conditions were applied at the external boundaries.

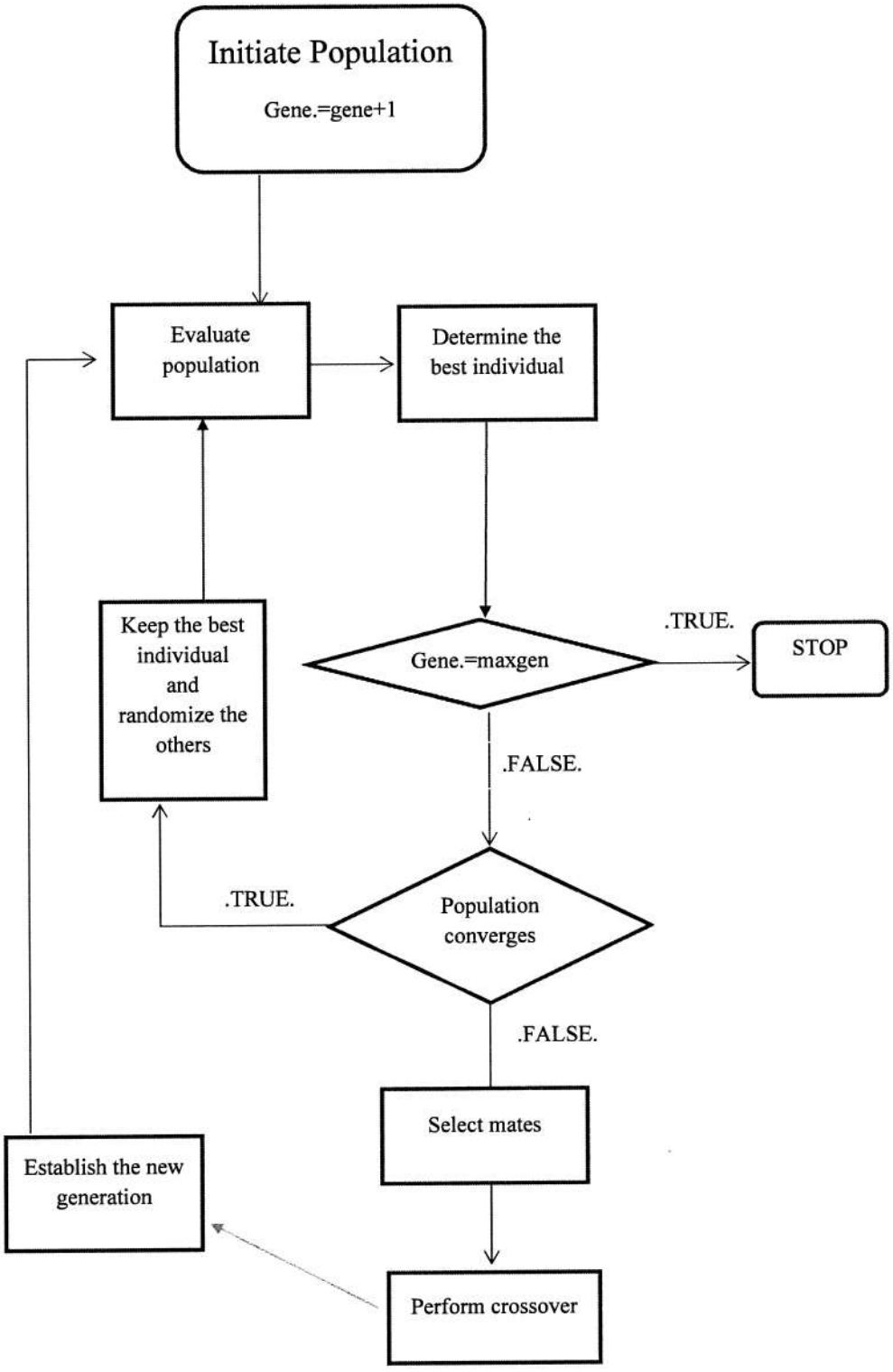

Figure 2. Flowchart of the optimization process:

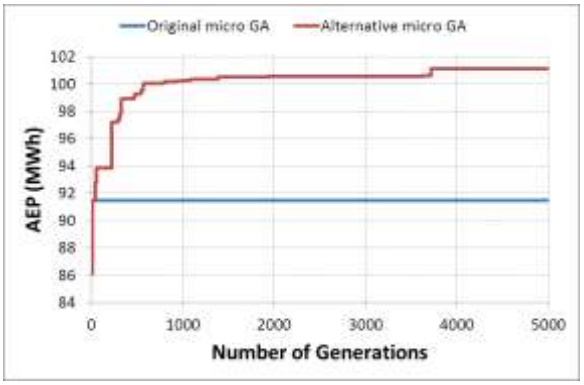

Figure 3. Evolution of AEP of a three-bladed turbine (P_{rated} = 30 kW) obtained using the original and alternative regeneration approach

In order to decide on the size of the mesh for CFD solutions, a grid independence study was performed. Here torque developed at a wind speed of 10 m/s without yaw error was computed using meshes consisting of 1.07 million, 1.87 million, 3.05 million and 3.41 million grid points. The external view and blade surface mesh along with periodic boundaries for the 3.41 million point case were displayed in Figure 3 and Figure 4. Spalart-Allmaras turbulence model was used in the computations. Results were displayed in Figure 5 where the predictions seemed to stabilize after a grid size of 3.05 million. Consequently, the mesh with 3.41 million points was adopted and used for the further CFD solutions.

Figure 3. External view of the mesh with 3.41 million points

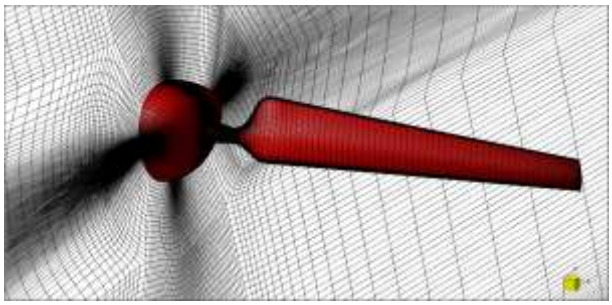

Figure 4. Surface mesh on blade and periodic boundaries (3.41 million points)

Torque predictions obtained using WT_Perf and CFD were displayed and compared with the experimental data (Simms et al. 2001) in Figure 6.

Analysis of Figure 6 showed that there are considerable discrepancies between computed and measured results. However, such discrepancies were also observed in the blind comparisons performed by NREL (Simms et al. 2001) and previous Navier-Stokes predictions (Sorensen et al. 2002). Among the CFD solutions, predictions with the k-ω SST model were considered to be the best.

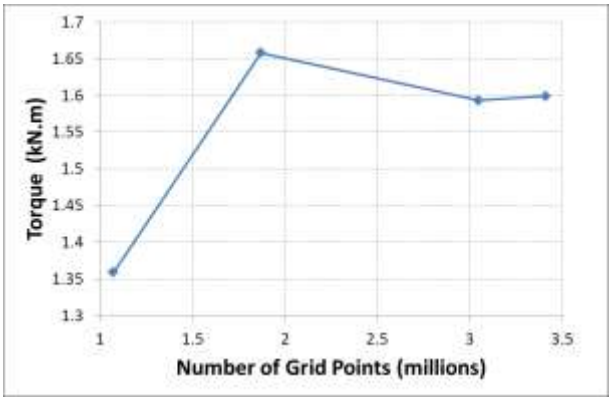

Figure 5. Torque predictions at 10 m/s of wind speed using different mesh sizes.

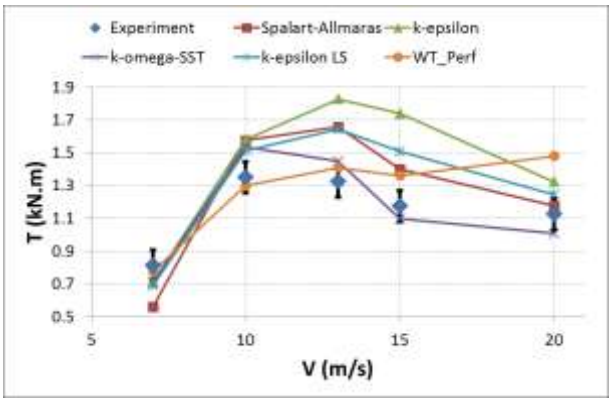

Figure 6. Shaft Torque of NREL Phase VI turbine.

Spalart-Allmaras model and low-Re k-ε model performed similarly while the predictions of the standard k-ε model were the worst. WT_Perf performed very well at wind speeds 7 m/s, 10 m/s and 13 m/s but the accuracy of its predictions decreased considerably as the wind speed increased. According to Weibull distribution for Gökçeada, the mean wind speed at this location is about 8.8 m/s. Therefore, WT_Perf could be used with confidence for this wind site. One interesting point was the solutions at 10 m/s where WT_Perf prediction was much better than the CFD solutions. This wind speed was at the onset of massive flow separation and unstable flow field imposed a difficult case for numerical solutions (Sorensen et al. 2002). This can be seen from Figure 7 where CFD predictions for skin friction lines on the suction surface of the blade at 10m/s wind speed were plotted. This solution was performed using k-ω SST turbulence model. Interestingly, WT_Perf seemed handled this case pretty well. However, when comparison of the local torque coefficient (C_q) predictions of WT_Perf with wind tunnel measurements, displayed in Figure 8 were examined, it was observed that WT_Perf under-predicts local torque

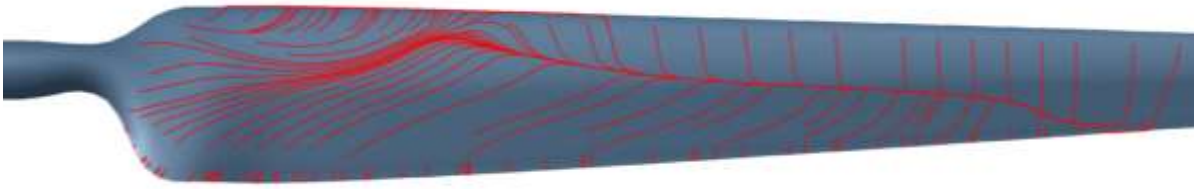

Figure 7. Skin-friction lines on the suction side of NREL Phase VI blade. (V = 10 m/s, k-ω SST turbulence model)

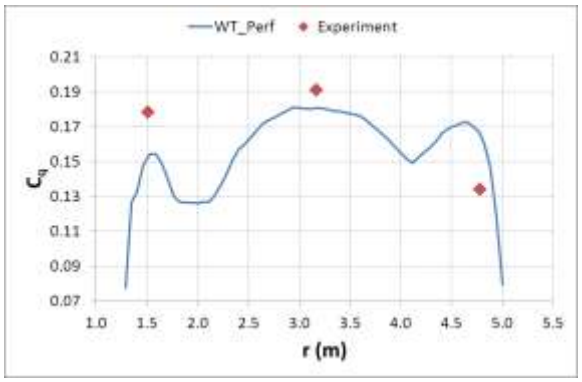

Figure 8. Distribution of local torque coefficient across the span of NREL Phase VI blade (V = 10m/s)

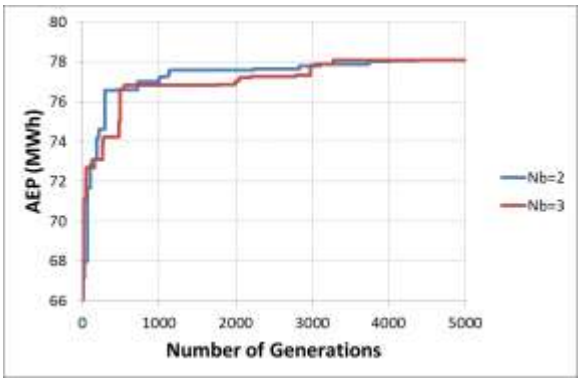

Figure 9. Evolution of AEP for 2 and 3 bladed turbines with 20 kW rated power

at the inner regions of the blade while it over-predicts this at the outer regions. Here, these discrepancies might have cancelled each other and thus led to good shaft torque predictions.

OPTIMIZATION RESULTS AND DISCUSSION

The optimization process was performed for turbines with rated power of 20 and 30 kW. Here, power output of the best turbine of a generation was not allowed to exceed 10% of the corresponding rated power. Two- and three-bladed configurations were optimized using a population size of five individuals. Cut-in and cut-out speeds of the turbine were set to be 4m/s and 25 m/s, respectively.

Optimizations were performed for 5000 generations. Figure 9 displays the evolution of AEP for 20 kW turbines with two and three blades. In this figure Nb stands for number of blades. Interestingly, optimized AEP of two and three bladed designs turned out to be nearly identical, which was approximately 78.085 MWh.

The AEP evolutions of 30 kW turbines were displayed in Figure 10 For this case the three-bladed configuration yielded an AEP of 101.107 MWh which was slightly larger than 99.811 MWh of the two-bladed configuration.

For the both rated power cases studied above, the energy production of two bladed turbines were very close to those of three-bladed turbines. As expected their power outputs, which were shown in Figure 11,

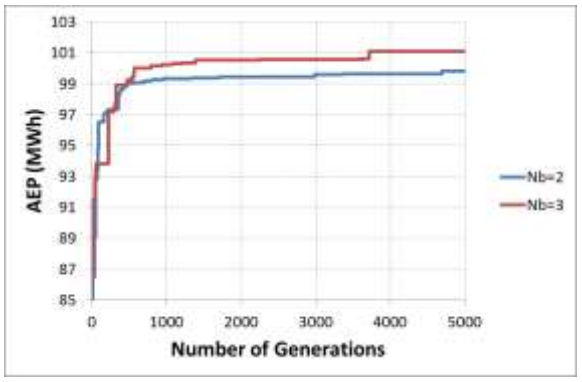

Figure 10. Evolution of AEP for 2 and 3 bladed turbines with 30 kW rated power

were also very close. 20 kW turbines stalled earlier than the 30 kW ones in order to limit their power output. According to this figure, the former turbines stalled at a wind speed of about 11 m/s while the latter ones stalled at approximately 12 m/s. Even this nearly 1 m/s difference in the rated wind speeds caused more than 20 % increase in the AEP. In order to see this increase, the energy capture curve, which is the power multiplied by the Weibull function ($W(V)$) versus wind velocity, was plotted in Figure 12. The integral of this curve times the number of hours in a year gives the AEP (without including the losses and efficiencies of the components). The Weibull distribution $W(V)$ was also included (dashed line) along with the mean wind speed of the wind site (vertical line) into this figure for reference. It was clear that without changing the diameter of the rotor, one could increase the energy capture by designing

the blades for a higher rated power. However, according to Figure 12, majority of the additional energy capture occurred when the turbine operated in stalled condition, where the performance would be more sensitive to changes in the wind conditions like yaw error, gust or turbulence. Moreover, a larger generator would be required for high rated power which might increase the cost of energy production.

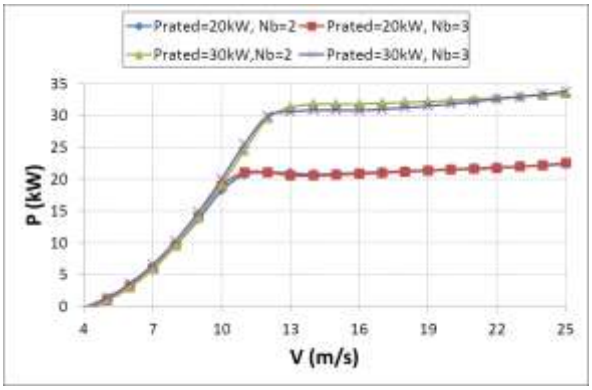

Figure 11. Power output of optimized turbines

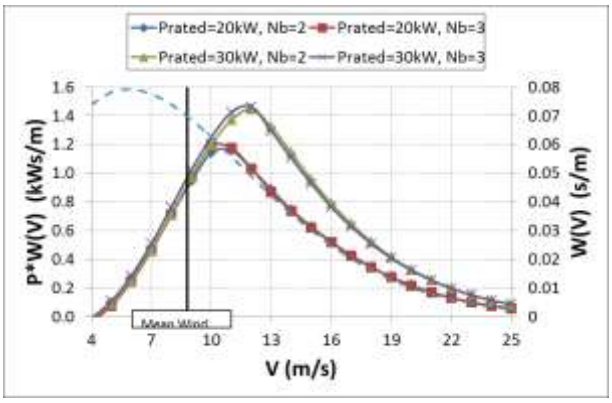

Figure 12. Energy capture curve

Two- and tree-bladed turbines with the same rated power yielded similar power outputs by having different design parameters. First of all, the optimum tip speed ratio (λ_{opt}), hence the rotation speed (ω), of two-bladed turbines was higher than that of three-bladed ones. The values were summarized in Table 2

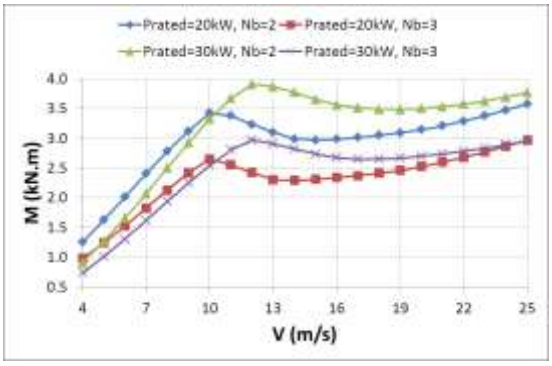

Figure 13. Flap-wise bending moments developed on the blades

Table 2. Optimum tip speed ratios and rotation speeds of the optimized turbines

Rated Power (kW)	Number of Blades	λ_{opt}	ω (rpm)
20	2	5.5	91.86
	3	5.0	83.51
30	2	6.5	108.56
	3	5.5	91.86

Increasing the rotation speed also generates some adverse effects. First it tends to increase the bending moment developing on the blades (Burton et al. 2001). Figure 13 shows the flapwise bending moments developed on the optimized blades at different wind speeds. Clearly, two-bladed turbines, which rotated faster than the three-bladed ones, were subjected to more bending loads at a given wind speed. Consequently, stronger blades would be required and cost of energy might increase. Power coefficient versus tip speed ratio curves, which indicates efficiency (Burton et al. 2001), of the rotors were displayed in Figure 14. The maximum Cp's of the turbines were close. Here, two-blade configurations were more efficient at high **λ** (low wind speed) while this situation was slightly reversed for low **λ** (high wind speed).

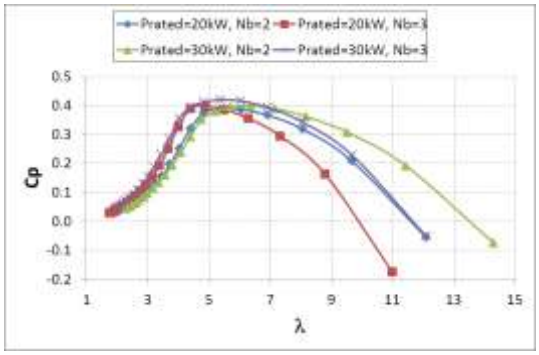

Figure 14. Cp vs λ curves of the optimized turbines

Airfoil profiles assigned to the root, primary and tip sections of the blades by the genetic algorithm were summarized in Table 3. For all configurations NACA 63-218 airfoil was used for the primary section of blades. This airfoil can be considered as a "well-performing" airfoil in terms of post-stall lift behavior and transition characteristics (Bertagnolio et al. 2001). For the root section, three of the four designs adopted S814 airfoil. This airfoil was designed for "insensitivity to roughness" and has been used as a root airfoil by NREL for turbines with a diameter of 10-15m (Tangler and Somers, 1995). The other root airfoil S823 is also a root airfoil suitable for small constant speed turbines (Tangler and Somers, 1995). For the tip region each design adopted a different airfoil section. Typically three-bladed turbines adopted airfoils with high maximum lift coefficient while the two-bladed ones adopted low maximum lift coefficient airfoils with somewhat smooth stall characteristics.

Table 3. Airfoil sections at the root, primary and tip section of the blades

Rated Power (kW)	Number of Blades	Root	Primary	Tip
20	2	S814	NACA 63-218	NACA 63-215
	3	S823	NACA 63-218	S834
30	2	S814	NACA 63-218	S809
	3	S814	NACA 63-218	E387

Blade twist distributions along the span were displayed in Figure 15 where pitch angle of a section was measured from the plane of rotation and was positive towards feather (towards oncoming wind). 20kW turbines had similar twist distributions and compared to the 30 kW turbines they were more twisted toward stall close to the tip region. This increased the local angle of attack and caused the blades stall at an early wind speed. This situation can be seen in Figure 16 where spanwise angle of attack distributions of three-bladed turbines were displayed. It is evident from this figure that the local angle of attack for a wind speed was higher for the low power turbine especially close to the tip region even though its rotation speed was higher than that of the high power one. One interesting situation observed in Figure 15 was the twist distribution of the two-bladed 30 kW turbine. This was not monotonically decreasing like the others. Comparison of angle of attack distributions the two 30 kW turbines in Figure 17 revealed that; at high wind speeds, lower lift characteristic of the S809 airfoil compared to the NACA 63-218 led to an increase in the angle of attack at the tip region of the two-bladed turbine. Twisting the blade toward feather prevented this angle rise too much. However, it also yielded a relatively complicated geometry which may be difficult to manufacture.

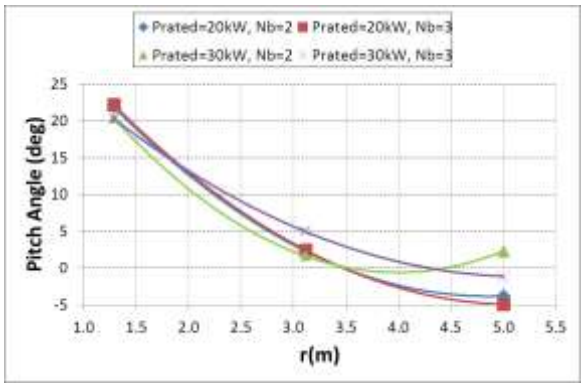

Figure 15. Spanwise twist distributions of the blades

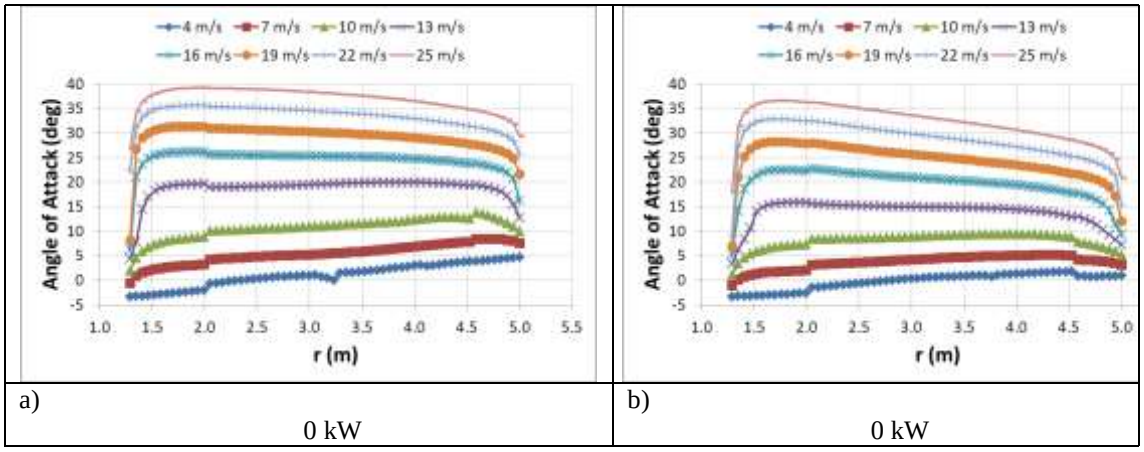

a) 0 kW b) 0 kW

Figure 16. Spanwise angle of attack distributions of three-bladed turbines at different wind speeds

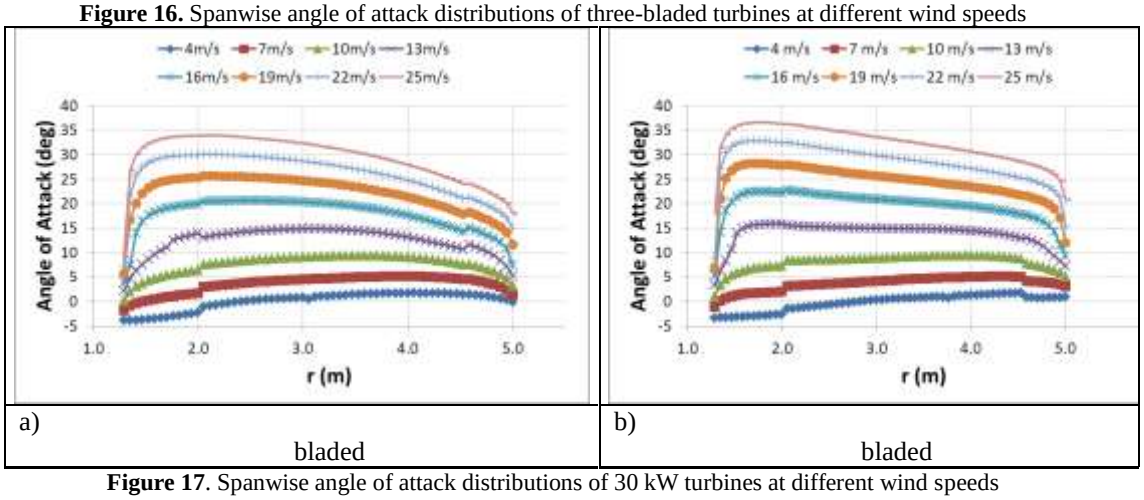

a) bladed b) bladed

Figure 17. Spanwise angle of attack distributions of 30 kW turbines at different wind speeds

Chord (c) distributions of the optimized blades were shown in Figure 18. According to this figure three-bladed configurations had thinner blades than 2 bladed ones. Typically thin blades have less bending strength; however this was offset by lower bending moments developed on three bladed rotors (see Figure 13). The resulting blade geometries were displayed in
Figure **19**. Despite having thinner blades, three-bladed configurations had higher chord solidity (σ_r) than two bladed rotors, which was displayed in
Figure **20**. Increasing solidity leads to an increase in the rotor thrust force (T) (Burton et al. 2001). This situation was shown in
Figure **21** for the turbines optimized in this study. Here three-bladed turbines produced a higher thrust force than the ones with two blades for both rated powers. However, thrust difference was lower for the 30 kW case. This was because the increase in the solidity for 30 kW case was lower than that of 20 kW case for the primary part of the blade. This situation can be observed from Figure **22** which showed that the difference between the solidities of two- and three-bladed turbines was almost uniform throughout the whole span for the 20kW case. On the other hand, 30 kW turbines had much higher solidity difference in the vicinity of the root and the tip regions while the difference was low at the primary section of the blade.

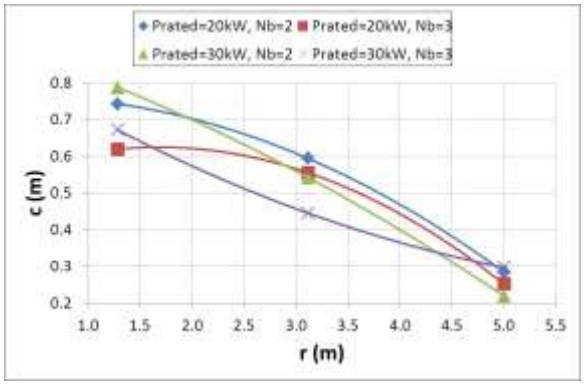

Figure 18. Spanwise chord distributions of the blades

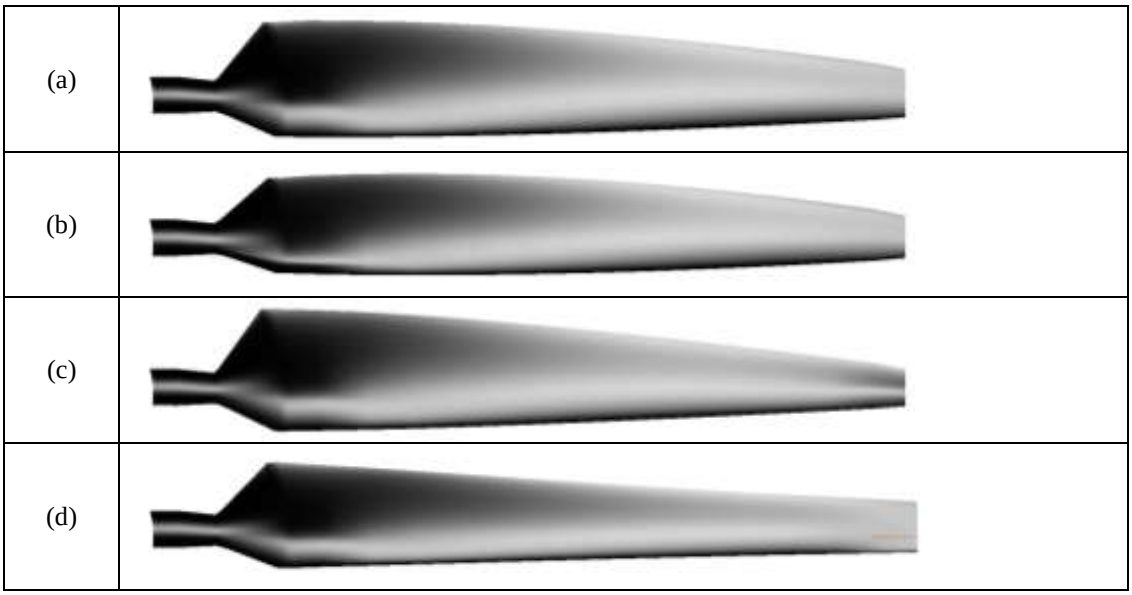

Figure 19. Blade geometries a) 20 kW rated power 2 blades, b) 20 kW rated power 3 blades c) 30 kW rated power 2 blades, d) 30 kW rated power 3 blades.

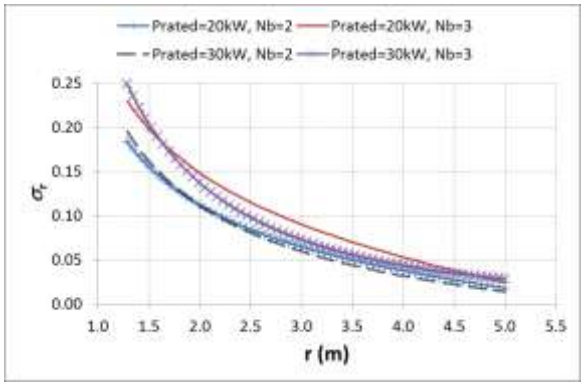

Figure 20. Chord solidities of the blades

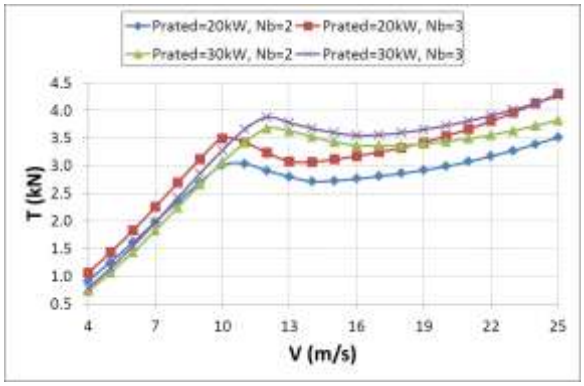

Figure 21. Thrust force developed on the rotors

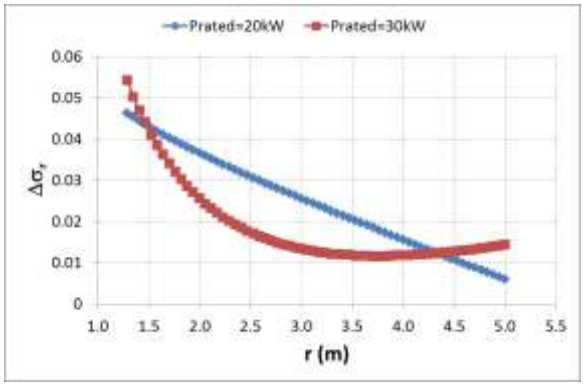

Figure 22. Difference between the chord solidities of two- and three-bladed configurations

CONCLUSIONS

Optimization studies of 10.6 m diameter, stall regulated and constant speed horizontal axis wind turbines were performed for Gökçeada, Turkey location using a genetic algorithm. Two- and three-bladed configurations were considered for 20kW and 30 kW rated power. For the optimization process AEP was used as the fitness function, which was calculated using a BEMT code WT_Perf. During the design process chord length and twist angle distributions along the blade span, airfoil sections for the root, primary and tip portions of the blade, and the pitch angle of the blades were used as design parameters. Three different airfoil databases for the three blade portions were generated. Aerodynamic data of the airfoils were mainly obtained from the available experimental data. However, when wind tunnel measurements in the desired Reynolds number range were not available, required aerodynamic data were generated using the XFLR5 software. Here, predictions were obtained using fixed transition to turbulence on upper and lower surfaces of the airfoil in order to include the roughness effect which typically occurs due to leading edge contamination. Numerical predictions for section lift and drag data of airfoils were obtained for angles of attack between 0 and 10 degrees and they were later extrapolated to the -180° - +180° angle of attack range using the preprocessor code AirfoilPrep developed by NREL. Optimization was performed using micro-genetic algorithm technique with tournament selection, uniform cross-over and elitist strategy where the best individual in the population was always carried on to the next generation. The population consisted of 5 turbines and optimization was performed for 5000 generations. The original micro genetic algorithm used did not apply mutation; instead the population was regenerated randomly if it has converged. However, this approach did not perform well in improving the best individual. Therefore, an alternative strategy was adopted, where the regeneration was being performed at every ten generations regardless of the convergence.

In order to validate the BEMT tool used in the computations, first a segment independence study was performed on the WT_Perf solutions, then shaft torque predictions for the NREL Phase VI turbine were compared with experimental measurements and CFD predictions obtained using different turbulence models. CFD solutions were obtained using the FINE-TURBO package of Numeca software. A grid independence study was performed for CFD solutions in order to select a suitable mesh size. Comparisons showed that BEMT solutions were accurate all the way to 13m/s of wind speed; however they showed considerable deviations from measurements beyond this speed. Nevertheless, considering the annual wind speed distribution for the turbine site, this performance was found to be sufficient. CFD predictions also showed deviations from measurements and the k-ω SST turbulence model performed relatively better than the others.

The optimization process was performed for two- and three-bladed turbines with rated power of 20 and 30 kW. Here, power output of the best turbine of a generation was not allowed to exceed 10% of the corresponding rated power. AEP predictions for the two- and three- bladed designs turned out to be very close. This was because genetic algorithm adjusted the design parameters such that both designs produced a similar power output. However, this caused the two-bladed rotors rotate faster and subject to heavier bending loads. On the other hand, optimized blades of the two-bladed configurations were thicker than the three-bladed ones especially at the root region and this was expected to provide more bending strength. Also Cp vs. λ curves of the rotors showed that two-bladed designs operate more efficiently at lower wind speeds and vice versa. In order not to exceed the imposed rated power constraint, 20 kW turbines stalled at a lower wind speed than the 30 kW designs. This caused the blades of the 20kW turbine be more twisted toward stall, especially at the outboard locations, in order to increase the local angle of attack.

Despite having thinner blades, three-bladed configurations had more solidity than two-bladed ones; hence they developed more thrust force. However, compared to the 20 kW case, thrust force difference between two-and three-bladed rotors of 30 kW case was lower. This was mainly attributed to the chord length distribution of the three-bladed 30 kW turbine, which had a convex shape unlike the other turbines having concave chord distributions. This convex distribution allowed it to have lower chord solidity at the primary section of the blade and thereby restricted the increase of the developed thrust force.

In the light of the discussions above, two-bladed configuration seemed to be preferable for 20 kW

rated power while a three-bladed rotor looked more suitable for 30kW.

ACKNOWLEDGEMENTS

This work was sponsored by Scientific Research Projects Commission of Marmara University, under the grant number FEN-A-060510-0136.

REFERENCES

Benjanirat, S. and Sankar, L. N., Evaluation of Turbulence Models for the Prediction of Wind Turbine Aerodynamics, *AIAA Paper, 2003-0517*, 2003.

Bertagnolio, F. Sorensen, N., Johansen, J., Fuglsang, P., Wind Turbine Airfoil Catalogue, *Riso-R-1280*, 2001.

Burton, T., Sharpe, D., Jenkins, N. and Bossanyi, E., *Wind Energy Handbook*, John Wiley & Sons, Ltd., 2001.

Ceyhan, O., Aerodynamic Design and Optimization of Horizontal Axis Wind Turbines by using BEM Theory and Genetic Algorithm, *MS Thesis*, Middle East Technical University, Ankara, Turkey, 2008.

Diaz-Casas, V., Becerra, J-A., Lopez-Pena, F. and Duro, R. J., Wind Turbine Design through Evolutionary Algorithms based on Surrogate CFD Methods, *Optimization Engineering*, DOI 10.1007/s11081-012-9187-1, 2012.

Duque, E.P., Burklund, M.D. and Johnson, W., Navier-Stokes and Comprehensive Analysis Performance Predictions of the NREL Phase VI Experiment, *Journal of Solar Energy Engineering*, 125, 457 – 467, 2003.

Eke, G. B. and Onyewuidala, J. I., Optimization of Wind Turbine Blades using Genetic Algorithm, *Global Journal of Researches in Engineering*, 10, 22. 2010.

FINE^{TM}/Turbo v8.7 User Manual, Numeca International, 2010.

Fuglsang, P. and Madsen, H. A., Optimization Method for Wind Turbine Rotors, *Journal of Wind Engineering and Industrial Aerodynamics*, 1, 191-206, 1999.

Fuglsang, P. and Thomsen, K.., Site-Specific Design Optimization of 1-5-2.0 MW Wind Turbines, *Journal of Solar Energy Engineering*, 123, 296 – 303, 2001.

Giguére, P. and Selig, M. S., Design of a Tapered and Twisted Blade for the NREL Combined Experiment Rotor, *NREL/SR-500-26173*, 1999.

Hansen, C., NWTC Computer-Aided Engineering Tools: AirfoilPrep, http://wind.nrel.gov/designcodes/preprocessors/airfoilprep/. Last modified 14 - December-2012.

Holst, T., Genetic Algorithms Applied to Multi-Objective Aerodynamic Shape Optimization, *NASA/TM – 2005-212846*, 2005.

http://wind.nrel.gov/airfoils/Coefficients/

http://wind.nrel.gov/designcodes/simulators/wtperf

http://www.cuaerospace.com/carroll/ga.html.

http://www.numeca.com/index.php?id=turbomachine

http://web.mit.edu/drela/Public/web/xfoil/

http://www.xflr5.com/xflr5.htm

IEC 61400-2, Wind Turbines – part 2: Design Requirements for Small Wind Turbines, IEC, 2006.

Kimilli, M. O., Erisik, A., Sahin, E. and Alpman, E., Horizontal Axis Wind Turbine Design Using Genetic Algoritm, *International Renewable Energy Conference*, IRENEC-059, 2012.

Launder, B. E. and Sharma, B. I., Application of the Energy-dissipation Model of Turbulence to the Calculation of Flow near a Spinning Disc, *Letters in Heat and Mass Transfer*, 1, 131 - 138, 1974.

Leishman, J. G., Challenges in Modelling the Unsteady Aerodynamics of Wind Turbines, *Wind Energy*, 5, 85 – 132, 2002.

Menter, F. R., Two-Equation Eddy-Viscosity Turbulence Models for Engineering Applications, *AIAA Journal*, 32, 1598 - 1605, 1994.

Sagol, E., Site Specific Design Optimization of a Horizontal Axis Wind Turbine based on Minimum cost of energy, *MS Thesis*, Middle East Technical University, Ankara, Turkey 2010.

Selig, M. S., Guglielmo, J. J., Broeren, A. P. and Giguere, P., *Summary of Low-Speed Airfoil Data: Volume I*, SolarTech Publications, 1995.

Selig, M. S. and McGranahan, B. D., Wind Tunnel Aerodynamic Tests of Six Airfoils for use in Small Wind Turbines, *NREL/SR-500-34515*, 2004.

Senecal, P. K., *Numerical Optimization using the GEN4 Micro-Genetic Algorithm Code*, Engine Research Center, University of Wisconsin-Madison, 2000.

Simms, D., Schreck, S., Hand, M. and Fingersh, L. J., NREL Unsteady Aerodynamics Experiment in the NASA-Ames Wind Tunnel: A Comparison of Predictions to Measurements. *NREL/TP-500-29494*, 2001.

Somers, D.M., The S822 and S823 Airfoils, *NREL/SR-500-36342*, 2005.

Sorensen, N. N., Michelsen, J. A. and Schreck, S., Navier-Stokes Predictions oft he NREL Phase VI Rotor in the NASA Ames 80ft x 120ft Wind Tunnel, *Wind Energy*, 5, 151 – 169, 2002.

Spalart, P. R. and Allmaras, S. R., A One-Equation Turbulence Model for Aerodynamic Flows, *AIAA Paper*, *92-0439*, 1992.

Tachos, N. S., Filios, A. E., Margaris, D. P. and Kaldellis, J. K., A Computational Aerodynamics Simulation of the NREL Phase II Rotor, *The Open Mechanical Engineering Journal*, 3, 9 – 16, 2009.

Tangler, J. L. and Somers, D. M., NREL Airfoil Families for HAWTs, *NREL/TP-442-7109*, 1995.

Weise, T., Global Optimization Algorithms - Theory and Application, available online (http://www.it-weise.de/), 2009.

WindPACT Blade System Design Studies, Innovative Design Approaches for Large Wind Turbine Blades, *Sandia Report*, *SAND 2003-0723*, 2003.

World Wind Energy Association, 2012 Small Wind World Report, 2012.